IEEE Access
Multidisciplinary | Rapid Review | Open Access Journal

Received August 10, 2019, accepted August 21, 2019, date of publication August 27, 2019, date of current version September 10, 2019.

Digital Object Identifier 10.1109/ACCESS.2019.2937897

Electromagnetic Performance Analysis on the Bearingless Permanent Magnet Synchronous Motor With Halbach Magnetized Rotor

TAO ZHANG[1,2], XIAOTING YE[1], LIHONG MO[1], AND QING LU[1]

[1]Faculty of Automation, Huaiyin Institute of Technology, Huai'an 223003, China
[2]Jiangsu Engineering Research Center on Meteorological Energy Using and Control, Nanjing University of Information Science and Technology, Nanjing 210044, China

Corresponding author: Xiaoting Ye (xiaotingye@163.com)

This work was supported in part by Natural Science Foundation of Jiangsu Province under Grant BK20181481, in part by the Postdoctoral Science Foundation of China under Grant 2017M610295, in part by the Six Categories Talent Peak of Jiangsu Province under Grant 2019-GDZB-238 and Grant 2016-GDZB-009, and in part by the Science and Technology Plan Projects of Huaian City under Grant HAB201832 and Grant HAP201903.

ABSTRACT In order to approximately obtain sinusoidal air-gap magnetic field and get larger radial levitation force of the bearingless permanent magnet synchronous motor (BPMSM), a novel BPMSM with Halbach magnetized rotor is proposed. Firstly, the suspension and rotation mechanisms of the BPMSM are introduced. The control mechanism of producing the radial levitation force in single direction and arbitrary direction is analyzed in detail. The mathematical models of the radial suspension force are given. Secondly, the comparative research on the BPMSMs with the Halbach magnetized rotor and parallel magnetized rotor is carried out. The air-gap magnetic field, back electromotive force (EMF), radial suspension force, and torque are calculated and compared. Finally, the prototype motor equipped with the Halbach magnetized rotor is constructed. Some experimental results are tested and the stable suspension operation of the proposed motor is realized.

INDEX TERMS Electric machines, permanent magnet machines, AC machines, magnetic levitation, magnetic circuits.

I. INTRODUCTION

High speed and high output power driving are the major development trends of electric machines. At present, high-speed electric machines are usually supported by ceramic bearings, whose life is 3-6 times longer than that of traditional mechanical bearings. However, it is far from enough to meet the performance requirements of high speed drive by improving the structure, material and lubrication conditions of mechanical bearings alone, especially the rotational speed of rotor exceeds 30000rpm. Therefore, lubrication of high-speed mechanical bearings has become the main factor affecting high-speed machining accuracy and service life of the motors. Moreover, non-contact hydrostatic bearings need to be equipped with pressure stabilization and strict filtration flow supply device, which leads to complex structure and large volume, and increases the cost of high-speed motors [1]. Magnetic bearings (MBs) are a new type of high performance bearings with no contact between rotor and stator by means of magnetic force. Moreover, the motor supported by MBs has some other advantages, such as no wear, no lubrication and sealing, no oil pollution, high speed, high accuracy, low noise, long life, and so on. They have the extremely important application value in the fields of high-speed precision CNC machine tool [2], [3], centrifuge [4], turbo-generator [5], turbine compressor [6], flywheel energy storage system [7]. However, the high-speed motor supported by magnetic bearings has obvious disadvantages, such as long axial length, low critical speed, high cost, low suspension force density and power density. Because the structure of the magnetic bearing is similar to that of the motor, the suspension winding of the magnetic bearing and the torque winding are embedded in the stator slot of the motor to form a bearingless motor. Torque and suspension force will be produced simultaneously in bearingless motors.

Bearingless motors have been studied for many applications such as the electrically-driven, flywheel energy storage, the milling tool, the centrifugal compressor, the gas

The associate editor coordinating the review of this article and approving it for publication was Xiaodong Sun.

turbine generator and turbo molecular pump [8], [9]. Various types of the bearingless motors have been introduced which combine a motor and a magnetic bearing [10], [11]. For example, bearingless permanent magnet motors, bearingless induction motors, bearingless switched reluctance motors. The bearingless reluctance motor has simple structure and low cost, but it has large torque fluctuation and mechanical vibration of rotor [12]–[15]. The bearingless induction motor has good high temperature resistance and can withstand large centrifugal force, but it has large rotor loss and low efficiency [16]–[18]. The bearingless permanent magnet motor can overcome the shortcomings of the two types of the above motors to some extent. It has high power and simple control [19]–[21]. These motors can support the rotors without any physical contact and have torque which replace the contact components and reduces the overall size [22]. In these types of bearingless motors, the BPMSMs have attracted considerable interests due to the advantages of the small size and light weight, the high power factor and efficiency, and no need excitation current in the main winding. Compared with permanent magnet synchronous motor, the structure and control of the BPMSM are very complex. Therefore, it is necessary to achieve high-speed operation of the BPMSM to show their technical advantages. But when the BPMSM operates at high speed, the air-gap magnetic field frequency can reach hundreds of Hertz or even higher [8], [23]. High-order harmonics in the air-gap magnetic field can lead to motor performance degradation, such as large torque ripple, levitation force ripple, loss and serious motor heating [24]–[28]. Furthermore, there is a tradeoff between the permanent magnet thickness (and, hence, torque density) and radial suspension force generation [29]–[31]. Thus, optimizing the magnetization of permanent magnets and reducing the harmonics in the air-gap magnetic field are of great significances to improve the performance of the BPMSM [7], [32]–[35].

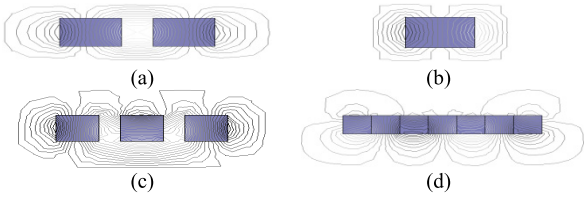

FIGURE 1. Magnetic field distribution.

The air-gap magnetic field is closely related to the magnetization of the rotor permanent magnets. Magnetization of the permanent magnet can be mainly classified as radial magnetization and parallel magnetization. Fig. 1(a) shows the magnetic field generated by two radial magnetized magnets, and the magnetic field produced by a parallel magnetized magnet is shown in Fig. 1(b). Moreover, magnetic field produced by one parallel magnetized magnet and two radial magnetized magnets is shown in Fig. 1(c). The fluxes are superimposed on each other. As a result, the flux is increased on one side and decreased on the other side. Magnetic field distribution of improved permanent magnets arrangement is shown in Fig. 1(d), which is called as Halbach planar array. In this topology, the effect of magnetic field superposition and attenuation is more obvious than that in Fig. 1(c).

The Halbach array can also be arranged into a curved surface, as shown in Fig.2. The magnetic field is enhanced on the side of air-gap but weakened on the other side. Thus, the thinner permanent magnet is required to generate the torque and radial suspension force.

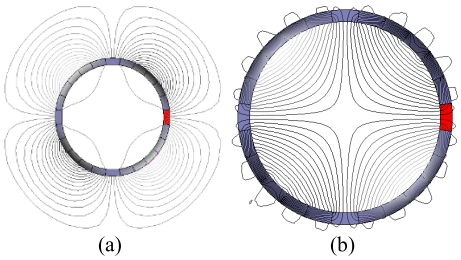

FIGURE 2. The 4-pole Halbach magnetized cylinder and field distributions.

Halbach array rotor offers many attractive features which can be effectively used in the motor design. One of the important characteristics is that it can cancel the flux on one side and strengthen on the other side [36]–[41]. Therefore, the rotor basically does not need a core, and can be hollow or nonmagnetic with very low rotational inertia. Furthermore, the air-gap magnetic field is near sinusoidal, which is important for improving the performances of the BPMSM.

In order to generate sinusoidal air-gap magnetic field waveform, improve the torque and radial suspension force density, a novel BPMSM with Halbach magnetized rotor is proposed in this paper. The suspension operation mechanism is analysed in detail [42]–[45]. The mathematical models of the radial suspension force are introduced. To illustrate the excellent performances of the proposed BPMSM, the comparative research on the BPMSM with parallel magnetized rotor is carried out with finite element method. The air-gap field distributions, back-EMFs, radial suspension forces, and torques are calculated and compared. The prototype motor equipped with Halbach magnetized rotor is designed and constructed [46]–[48]. Finally, the stable suspension operation of the proposed BPMSM is realized.

II. CONTROL MECHANISMS AND MATHEMATICAL MODELS

A. PRODUCING MECHANISM OF THE RADIAL SUSPENSION FORCE AND TORQUE

Fig. 3 depicts the mechanisms of the radial suspension force and torque in a BPMSM with 4-pole torque windings and 2-pole suspension windings. The torque is generated by the interaction of the 4-pole rotor magnetic field and 4-pole torque windings magnetic field, as shown in Fig. 3(a). Adding an additional suspension winding into the stator slots, the 2-pole suspension windings magnetic field will be generated. The radial suspension force is produced by the interaction of

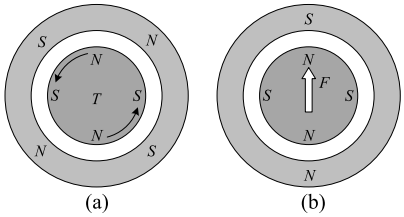

FIGURE 3. Producing mechanism of the torque and radial suspension force in a BPMSM with 4-pole torque windings and 2-pole suspension windings.

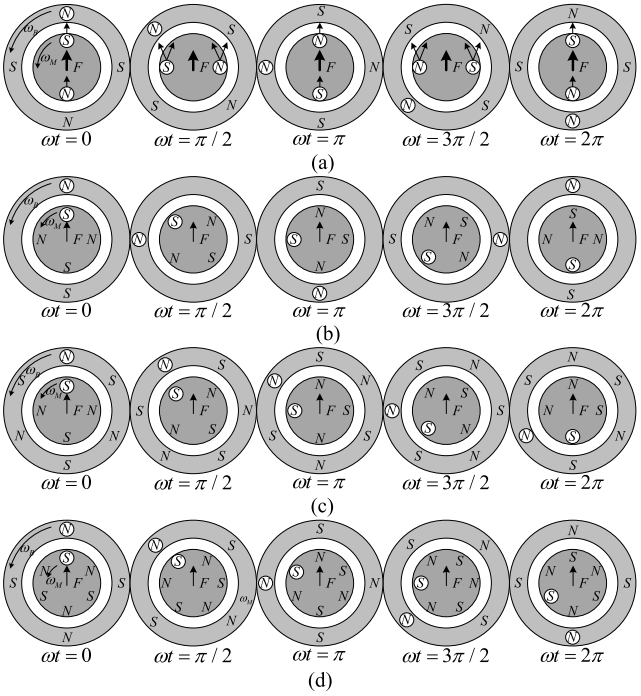

FIGURE 4. Radial suspension force control in single direction, (a) PM = 1, PB = 2, (b) PM = 2, PB = 1, (c) PM = 2, PB = 3, and (d) PM = 3, PB = 2.

the 2-pole magnetic field and 4-pole magnetic field, as shown in Fig. 3(b), which the north pole of the rotor and the south pole of the stator attract each other in the upper part of the motor while the two opposing north poles in the lower half will repel each other. As a result, a vertical resultant radial suspension force F is generated.

In brief, the radial suspension force can be generated in the BPMSM with P_{M} pole pair number, if an additional suspension winding with $P_{\mathrm{B}} = P_{\mathrm{M}} \pm 1$ pole pair number is added into the stator slots. This radial suspension force is used to provide a non-contact suspension for the rotor.

B. RADIAL SUSPENSION FORCE CONTROL IN SINGLE DIRECTION

Fig. 4 shows the control mechanism of the radial suspension force in a single direction when the motor rotates. The torque windings magnetic field and the rotor permanent magnet field can be equivalent each other [26]. Therefore, for simplicity, the torque windings magnetic field and rotor permanent magnet magnetic field can be viewed as a whole. At the same time, Fig. 4(a) is taken as an example to analysis because the same conclusions can be obtained from Fig. 4(b), Fig. 4(c), and Fig. 4(d).

In Fig. 4(a), when $\omega t = 0$, the south pole of the rotor and north pole of the stator attract each other in the upper part of the motor while the north pole of the rotor and north pole of the stator repel each other in the lower part. But when $\omega t = \pi/2$, the south pole of the rotor and left upper north pole of the stator attract each other, while the south pole of the rotor and left lower south pole of the stator repel each other in the left part of the motor. At the same time, the north pole of the rotor and right upper south pole of the stator attract each other, while the north pole of the rotor and right lower north pole of the stator repel each other in the right part of the motor. The electromagnetic force of each pole is shown as the thin lines with arrow. Consequently, a vertical resultant radial suspension force F is also generated and displayed as the thick line with arrow. The same method is adopted for the analysis of the mechanism of the single directional radial suspension force generation when $\omega t = \pi$, $\omega t = 3\pi/2$, and $\omega t = 2\pi$.

From above analysis, to generate the radial suspension force in a single direction, the rotation direction of the torque windings magnetic field and suspension windings magnetic field must be the same, and the mechanical angular velocities of two magnetic fields must satisfy the following condition.

$$P_M \omega_M = P_B \omega_B = \omega \tag{1}$$

where ω_M and ω_B are the rotation mechanical angular velocity of the torque windings magnetic field and suspension windings magnetic field, respectively. ω is the electrical angular velocity.

C. RADIAL SUSPENSION FORCE CONTROL IN ANY DIRECTION

To control rotor to realize stable suspension, BPMSMs need to generate the radial suspension force in any direction. Four types of BPMSM with different pole pair number have been investigated, as shown in Fig. 5, to analysis the necessary conditions for producing the radial suspension force in any direction.

According to (1), relative mechanical angular velocity $\Delta\omega$ between suspension winding magnetic field and torque winding magnetic field are expressed as

$$\Delta\omega = (\omega_B - \omega_M) = \omega\,(P_M - P_B)\,/P_M P_B \tag{2}$$

When $P_{\mathrm{M}} = P_{\mathrm{B}} - 1$, relative motion relationships between radial suspension force direction θ and relative mechanical angular velocity $\Delta\omega$, as shown in Fig. 5(a) and Fig. 5(c), are obtained as

$$\theta = P_B \Delta\omega \tag{3}$$

When $P_{\mathrm{M}} = P_{\mathrm{B}} + 1$, relative motion relationships between radial suspension force direction θ and relative mechanical

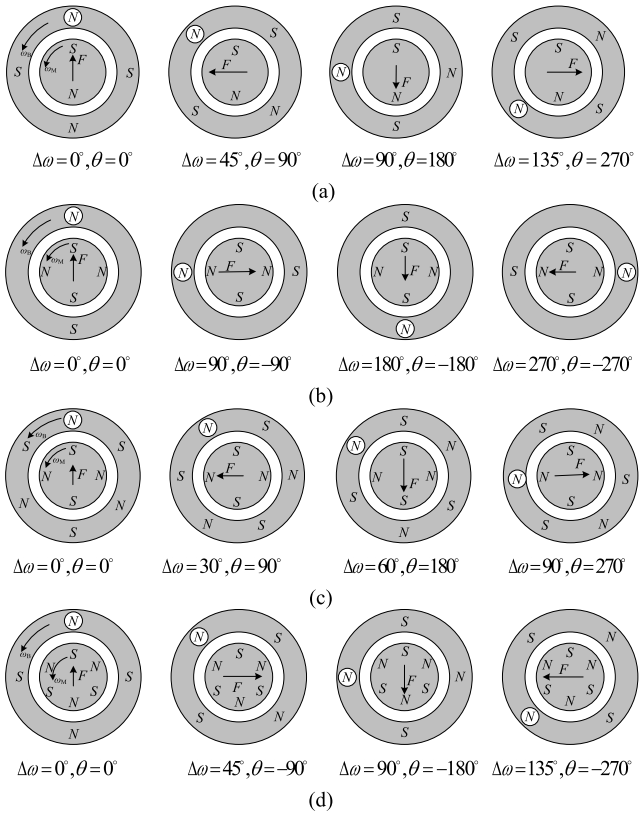

FIGURE 5. Radial suspension force control in any direction, (a) PM = 1, PB = 2, (b) PM = 2, PB = 1, (c) PM = 2, PB = 3, and (d) PM = 3, PB = 2.

angular velocity $\Delta\omega$, as shown in Fig. 5(b) and Fig. 5(d), are given a

$$\theta = -P_B \Delta\omega \tag{4}$$

Therefore, the conclusions can be obtained from above analysis. When the radial load is changing, BPMSM must be able to generate the radial suspension force in any direction to pull the rotor back to equilibrium position. From (3) and (4), the radial suspension force points toward the angle θ. The θ can be obtained as

$$\theta = (P_B - P_M) P_B \Delta\omega \tag{5}$$

In fact, suspension winding magnetic field is generated by the currents of the suspension windings, and torque winding magnetic field is generated by the currents of torque windings. According to the relationships between magnetic fields and currents in two sets of three phase symmetric winding, necessary conditions for generating the radial suspension force in any direction is that the current electric angular frequency of two windings must be equal. The direction of resultant radial suspension force is pointed to the initial phase difference between the two winding currents, namely, the angle θ expressed as (3), (4) and (5).

D. MATHEMATICAL MODELS

According to reference [17], [26], the mathematical models of radial suspension force in surface-mounted BPMSMs are expressed as following

$$\begin{cases} \begin{bmatrix} F_x \\ F_y \end{bmatrix} = M' I_p \sqrt{1 + \dfrac{I_q^2}{I_p^2}} \\ \quad \begin{bmatrix} -\cos(2\omega t + \theta) & \sin(2\omega t + \theta) \\ \sin(2\omega t + \theta) & \cos(2\omega t + \theta) \end{bmatrix} \begin{bmatrix} i_x \\ i_y \end{bmatrix} \\ I_p = \dfrac{8 B_r}{\pi \mu_0 n_4} l_m \\ M' = \dfrac{\mu_0 \pi n_2 n_4 l}{8} \times \dfrac{r - (l_m + l_g)}{(l_m + l_g)^2} \end{cases} \tag{6}$$

where I_p is the equivalent current of the permanent magnet. M' is the rate of change of the mutual inductances between the torque and suspension windings with respect to the rotor radial displacement. Specifically, M' is the partial differential value of the mutual inductances between torque and suspension windings with respect to the rotor radial displacements x and y. The unit of M' is H/m. I_q is the equivalent current of torque windings. n_2 and n_4 are the effective numbers of turns of the suspension and torque windings, respectively; l, l_m and l_g are the stack length of the rotor iron core, thickness of magnet and air-gap length, respectively. r is the inner radius of the stator iron core. It can be seen that the radial suspension forces are proportional to M' and I_p. If $M' \cdot I_p$ is large, radial suspension force winding currents i_x and i_y can be small. I_p is increased with the thickness of the permanent magnet. However, since the air-gap length between the rotor and stator iron cores is increased, it can be understood that M' is decreased. Accordingly, it can be expected that there is an optimal value of the permanent magnet thickness. Therefore, in the case of the given permanent magnet thickness, we expect to obtain a larger air-gap magnetic flux density.

III. AIR-GAP MAGNETIC FIELD OPTIMIZATION

A. BASIC PARAMETERS OF BPMSM

Permanent magnet rotors consist of buried permanent magnet rotor and surface-mounted permanent magnet rotor. Especially surface-mounted permanent magnet rotor is preferred which can endure the higher speed [20]. In this topology, magnets are glued on the rotor surface and fixed by a bandage. But this motor has long equivalent air-gap length for the bandage. Thus, the accurate calculations of suspension forces are especially important to suspension control of the BPMSM. The parameters of prototype motor are shown in Table 1.

B. DISTRIBUTION OF STATOR WINDINGS

According to fundamental parameters of BPMSM, static finite element analysis is carried out in this paragraph. The model of finite element analysis is constructed, as shown in Fig. 6(a), and the diagram of windings distribution is given in Fig. 6(b). The stator slots are divided into two layers. Torque windings are embedded into the outer layer with the phase sequence of X→Y→Z, and the pole pair number is two.

TABLE 1. Basic parameters of BPMSM.

Quantity	Value
Rated power	2500W
Axial length	85mm
Stator slots number	24
Out diameter of stator	12mm
Inner diameter of stator	67mm
Air-gap length	1mm
Permanent magnet thickness	2mm
Residual magnetic flux density	1.2T
Turn number of levitation coil	30
Turn number of torque coil	35
Coercive force	900kA/m

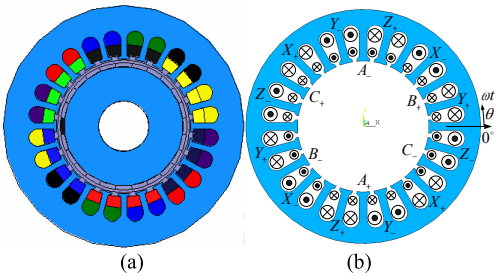

FIGURE 6. Diagram of finite element model and winding distribution.

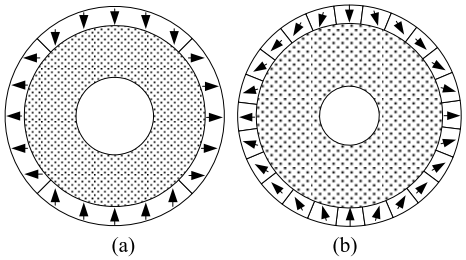

FIGURE 7. Structure of permanent magnet rotor. (a) Parallel magnetization. (b) Halbach magnetization.

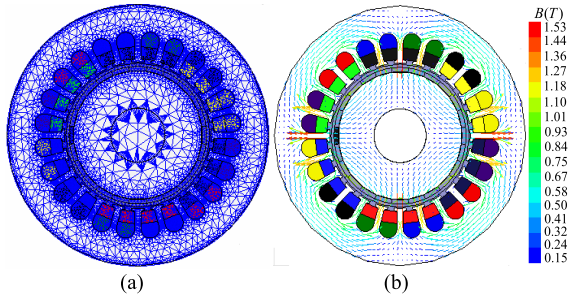

FIGURE 8. Diagrams of mesh division and magnetic field distribution.

Additional suspension windings are inserted into the inner layer with the phase sequence of A→B→C, and the pole pair number is one. Three phase symmetrical currents are applied to the two sets of windings simultaneously. And thus, two counter-clockwise rotational magnetic fields are produced, and the resultant radial suspension force is pointed to the positive direction of x-axis when two currents have the same initial phases.

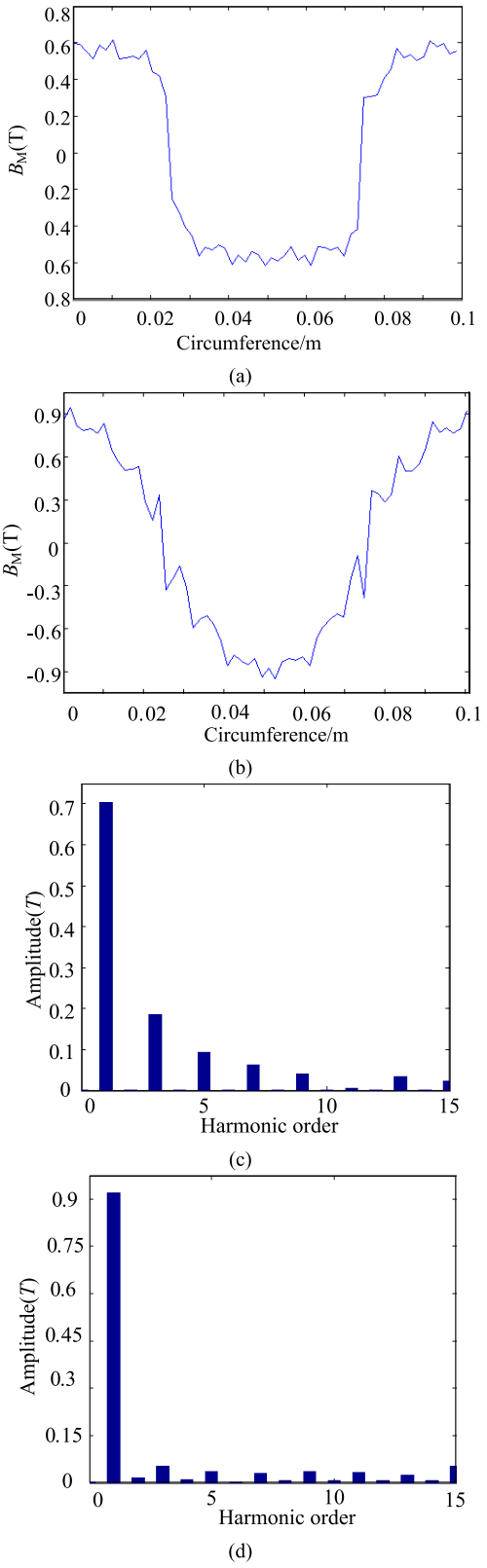

FIGURE 9. Air-gap magnetic field waveform and harmonics analysis. (a) Air-gap magnetic field with parallel magnetization, (b) air-gap magnetic field with Halbach array magnetization, (c) harmonics analysis with parallel magnetization, and (d) harmonics analysis with Halbach array magnetization.

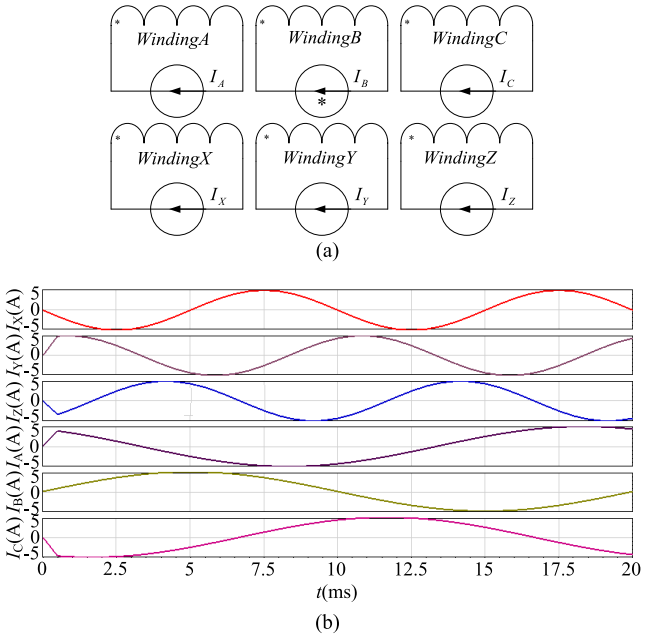

FIGURE 10. Diagrams of external circuits and currents, (a) external circuits and (b) waveforms of current source.

C. MAGNETIZED MODE OF MAGNETS

Fig. 7 shows two kinds of surface-mounted permanent magnet rotors. In Fig. 7(a), rotor permanent magnet ring is composed of four magnets, and each magnet adopts parallel magnetized mode. But in Fig. 7(b), the magnet ring consists of twenty-four magnets, and the Halbach magnetization is chosen to optimize the performances of the motor.

D. AIR-GAP MAGNETIC FIELD

Adaptive mesh division technology is used to mesh the finite element model. The diagram of mesh model is shown in Fig. 8(a). When no current is applied to both windings, the distribution of permanent magnetic field is shown in Fig. 8 (b). It can be seen that the four-pole symmetric magnetic field is generated by the permanent magnets. The maximum magnetic flux density reaches to 1.53T in the stator teeth, but magnetic flux density in the stator yoke is approximately 1T.

Air-gap magnetic flux density data are extracted from the established models, and Fast Fourier Transform is conducted. The analysis results are shown in Fig. 9. In Fig. 9(a), the air-gap magnetic flux density waveform is close to the rectangular wave with rich high order harmonics. The fundamental amplitude is approximately 0.7T, as shown in Fig. 9(c). But in Fig. 9(b), the waveform of air-gap magnetic flux density is a sine wave with less high harmonic contents, and its fundamental amplitude is 0.9T as shown in Fig. 9(d).

IV. TRANSIENT ANALYSIS CALCULATION

In this paragraph, the coupled external circuits are adopted, and the time stepping finite element method is used to analyze BPMSM considering the rotor rotation. The operating characteristics of the motor are simulated under various working conditions, and the transient parameters, such as back-EMF, radial suspension force, torque, are calculated and compared.

A. EXTERNAL CIRCUITS

The current source models are adopted to ignore the end effect. Fig. 10(a) shows the diagrams of external circuits which winding A, B, C and winding X, Y, Z are the external circuits of three-phase suspension windings and torque windings, respectively. According to the necessary conditions of producing stable and controllable radial suspension force, three phase symmetrical currents, as shown in Fig. 10(b), are applied to two sets of windings simultaneously. The frequencies of suspension winding currents and torque winding currents are 200 Hz and100 Hz, respectively. The current amplitude is 5 A. The initial phase difference θ is $-135°$. The rotating mechanical angular velocity of the rotor is set to 3000 r/min, and the computation time is given from 0 to 0.2 s. The time step size is configured to 0.001 s.

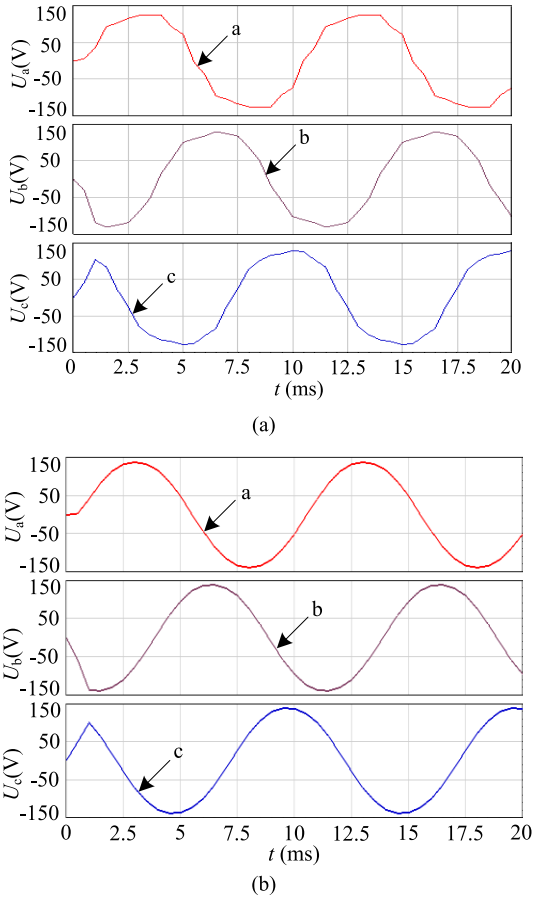

FIGURE 11. Back-EMF waveforms of torque windings, (a) parallel magnetization and (b) Halbach magnetization.

B. NO-LOAD BACK-EMF

Fig. 11 shows the no-load back-EMF waveforms when the rotor is rotating in the geometric center position. It can be seen that the back-EMF frequency of torque winding currents is 100 Hz. In Fig. 11(a), the amplitude of back-EMF

waveforms is 133 V. But in Fig. 11(b), the amplitude of back-EMF waveforms is 142 V for the larger air-gap flux density. Moreover, the back-EMF waveform of the motor with Halbach magnetized rotor is much more sinusoidal than the motor with the parallel magnetized rotor.

C. TRANSIENT SUSPENSION FORCE

Fig. 12 shows the transient radial suspension force waveforms. It can be seen that the force F_x is always equal to negative F_y because the direction of resultant radial suspension force is pointed to the angle θ. Thus, radial suspension force control mechanisms in a single direction and in any direction are all proved to be correct.

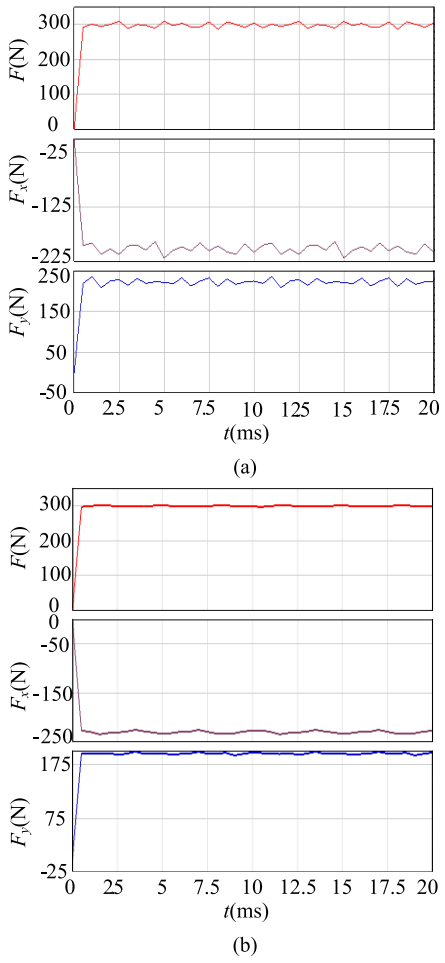

FIGURE 12. Radial suspension force waveforms. (a) Parallel magnetized mode and (b) Halbach magnetized mode.

The resultant radial suspension force waveform is fluctuant from 280 to 300 N, as shown in Fig. 12(a), and its average value is 287 N. In Fig. 12(b), the radial suspension force is approximately 300 N, and suspension force per unit current is 60 N. Moreover, the radial suspension force ripples of the motor with radial magnetized rotor are much larger than that with Halbach magnetized rotor.

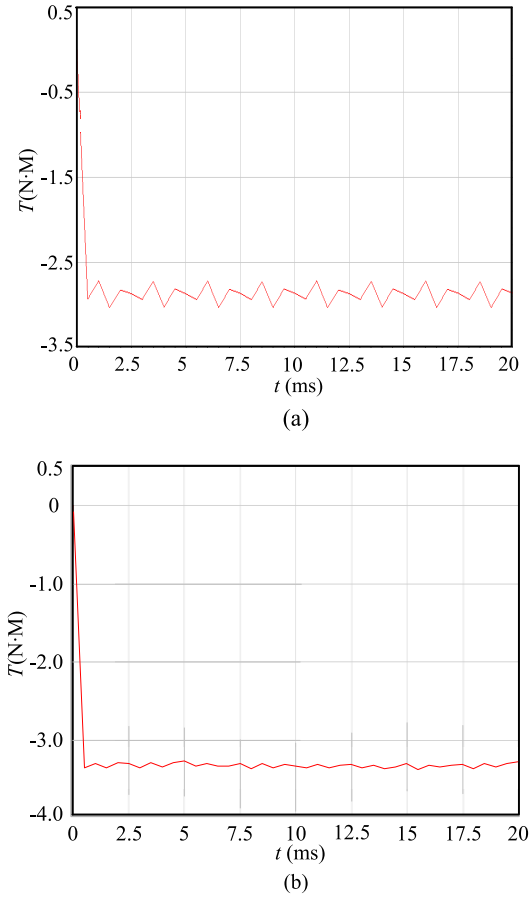

FIGURE 13. Waveform of torques. (a) Parallel magnetized rotor and (b) Halbach magnetized rotor.

D. TORQUE

Fig. 13 shows the transient torque waveforms. The torque amplitude is approximately 2.87 Nm in Fig. 13(a), but it is 3.3 Nm in Fig. 13(b), which is 15% larger than the former one for the large air-gap magnetic flux density. Moreover, the torque ripples in Fig. 13(a) is significantly larger than that in Fig. 13(b).

V. EXPERIMENTAL RESULTS

The control system of BPMSM consists of two basic parts, namely, speed control subsystem and radial displacement control subsystem, and its control block diagram is shown in Fig. 14.

Based on the radial shaft position, suspension force command F_x^* and F_y^* are generated from the radial position regulators in radial displacement control subsystem. The 2-pole suspension winding current commands are generated through the PARK and CLARK transformation. A current regulator, i.e., a current-controlled inverter, regulates the 3-phase currents.

In speed control subsystem, there is a rotary encoder on the rotor shaft, which is used to detect the instantaneous rotor angular position and the rotational speed. The detected

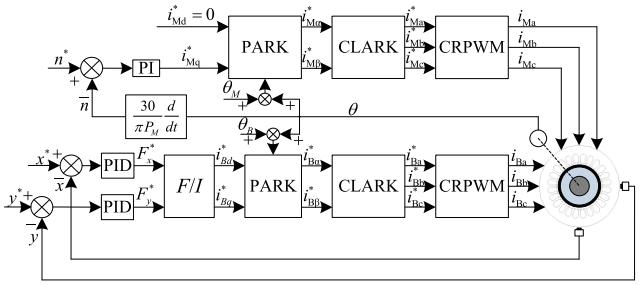

FIGURE 14. Control block diagram of BPMSM.

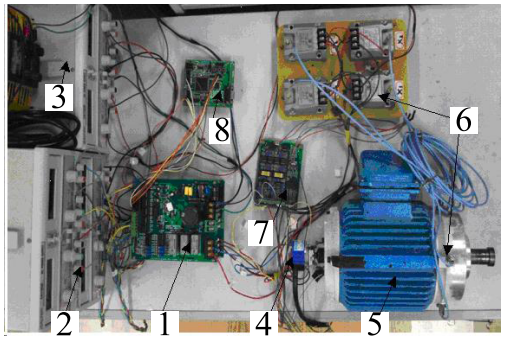

FIGURE 15. Experimental prototype BPMSM and platform. 1. Inverter, 2. direct current power supply, 3. alternating current power supply, 4. rotary encoder, 5. BPMSM, 6. displacement sensor, 7. interface circuit, and 8. controller.

speed is compared with its command and the q-axis motor current command i^*_{Mq} is generated via the speed regulator. Note that the d-axis motor current command i^*_{Md} is zero. The 2-phase and 3-phase current commands are generated, and a current regulator provides instantaneous regulation of the torque winding currents.

To verify the effectiveness of the proposed BPMSM with Halbach magnetized rotor and theoretical analysis, a two degrees of freedom experimental prototype motor and platform, as shown in Fig. 15, are built and tested. Some critical parameters of experimental prototype motor are given in Table 1.

The d-axis of the rotor is positioned at 0° by six steps positioning method. Then, rotor field oriented control program is executed. The given velocity is $n^* = 1200$r/min. The waveforms of given velocity commands and feedback velocity are shown in Fig. 16(a). It can be seen that the rotor rotational speed can quickly track the given speed signal, and speed waveform changes smoothly. The required time is 1.25 s to accelerate from standstill to the given speed.

Fig. 16(b) shows the tracking curve of rotor position angle in the stable suspension state. The feedback value of position angle can be quickly and accurately following the given value, which proves the correctness of the closed-loop control.

Fig. 16(c) shows the waveforms of B-phase suspension winding current and Y-phase torque winding current. The two current waveforms are all approximated as the sine waves, but there are certain harmonic components.

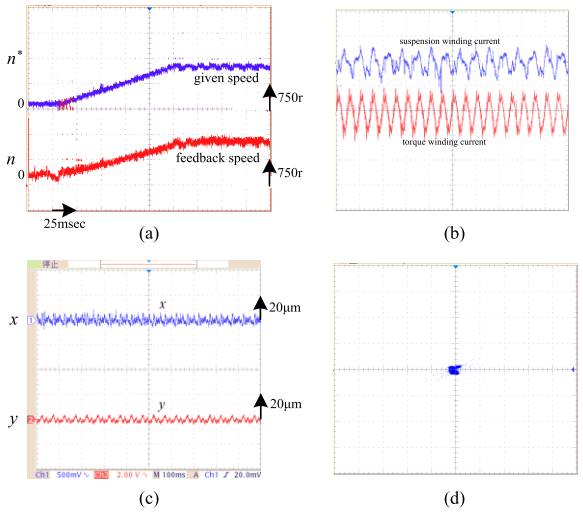

FIGURE 16. Experimental results, (a) given and feedback speed waveforms at startup, (b) given and feedback values of position angle, (c) current waveforms, (d) acceleration and deceleration experimental waveforms, (e) radial displacements in x and y direction, and (f) rotor trajectory diagram.

Acceleration and deceleration tests have been made, and the corresponding speed waveforms are shown in Fig. 16(d). The acceleration process time is approximately 0.19 s, but deceleration time is about 0.20 s. The BPMSM has good dynamic response performance.

Fig. 16(e) shows the radial displacements in x- and y-direction, and Fig. 16(f) gives the rotor trajectory diagram. From the experimental results, the BPMSM proposed in this paper can rotate and suspend the rotor stably, and the vibration amplitude of the rotor radial displacement is about 25 μm.

VI. CONCLUSION

According to the excellent properties of Halbach permanent magnet array, a BPMSM with Halbach magnetized rotor is proposed in this paper. The generation principles of torque and radial suspension force are discussed and analysed. Using finite element method, BPMSMs with two different permanent magnet rotors are studied. Radial suspension force, torque, and back-EMF are calculated and compared. An experimental prototype motor and platform are established and tested to verify the effectiveness of the proposed BPMSM and theoretical analysis. The conclusions are given as follows:

(1) The radial suspension force direction of BPMSM is pointed to the initial phase angle difference θ.
(2) BPMSM with Halbach array rotor has sinusoidal air-gap magnetic field and back-EMF.
(3) The radial suspension force generated by the BPMSM with Halbach array rotor is 1.034 times as much as the force produced by BPMSM with the parallel magnetized rotor, and the fluctuation of the radial suspension force is small.

(4) The torque of BPMSM with Halbach array rotor is 1.15 times as much as the torque produced by BPMSM with the parallel magnetized rotor, and the torque ripples are very small.

REFERENCES

[1] I. Arredondo and J. Jugo, "Precise positioning of an AMB spindle using 2-DOF controller," in *Proc. 10th Eur. Control Conf.*, Budapest, Hungary, Aug. 2014, pp. 1818–1823.

[2] S. Y. Yoon, Z. Lin, and P. E. Allaire, "On the control of single stage centrifugal compressor surge with active magnetic bearings," in *Proc. 13th Int. Symp. Magn. Bearings*, Arlington, VA, USA, 2012, pp. 1–11.

[3] F. C. Rosa, F. Lima, and M. A. Fumagalli, "Development of a high-speed turbo-generator supported by active magnetic bearings," in *Proc. 38th Annu. Conf. IEEE Ind. Electron. Soc.*, Montreal, QC, Canada, Oct. 2012, pp. 2232–2237.

[4] J. Asama, R. Natsume, H. Fukuhara, T. Oiwa, and A. Chiba, "Optimal suspension winding configuration in a homo-polar bearingless motor," *IEEE Trans. Magn.*, vol. 48, no. 11, pp. 2973–2976, Nov. 2012.

[5] H. Mitterhofer, W. Gruber, and W. Amrhein, "On the high speed capacity of bearingless drives," *IEEE Trans. Ind. Electron.*, vol. 61, no. 6, pp. 3119–3126, Jun. 2014.

[6] Y. Asano, A. Mizuguchi, M. Amada, J. Asama, A. Chiba, M. Ooshima, M. Takemoto, T. Fukao, O. Ichikawa, and D. G. Dorrell, "Development of a four-axis actively controlled consequent-pole-type bearingless motor," *IEEE Trans. Ind. Appl.*, vol. 45, no. 4, pp. 1378–1386, Jul./Aug. 2009.

[7] X. Sun, L. Chen, and Z. Yang, "Overview of bearingless permanent-magnet synchronous motors," *IEEE Trans. Ind. Electron.*, vol. 60, no. 12, pp. 5528–5538, Dec. 2013.

[8] X. Sun, Z. Jin, S. Wang, Z. Yang, K. Li, Y. Fan, and L. Chen, "Performance improvement of torque and suspension force for a novel five-phase BFSPM machine for flywheel energy storage systems," *IEEE Trans. Appl. Supercond.*, vol. 29, no. 2, Mar. 2019, Art. no. 0601505.

[9] P.-K. Budig, "Magnetic bearings and some new applications," in *Proc. 3th Int. Students Conf. Electrodyn. Mechatronics*, Opole, Poland, Sep. 2010, pp. 1–7.

[10] X. Sun, K. Diao, G. Lei, Y. Guo, and J. Zhu, "Study on segmented-rotor switched reluctance motors with different rotor pole numbers for BSG system of hybrid electric vehicles," *IEEE Trans. Veh. Technol.*, vol. 68, no. 6, pp. 5537–5547, Jun. 2019.

[11] K. Kang and A. Palazzolo, "Homopolar magnetic bearing saturation effects on rotating machinery vibration," *IEEE Trans. Magn.*, vol. 48, no. 6, pp. 1984–1994, Jun. 2012.

[12] T. Hentati, A. Bouaziz, S. Bouaziz, J.-Y. Choley, and M. Haddar, "Dynamic behaviour of active magnetic bearings spindle in high-speed domain," *Int. J. Mechtron. Manuf. Syst.*, vol. 6, nos. 5–6, pp. 474–492, 2013.

[13] X. Sun, K. Diao, G. Lei, Y. Guo, and J. Zhu, "Real-time HIL emulation for a segmented-rotor switched reluctance motor using a new magnetic equivalent circuit," *IEEE Trans. Power Electron.*, to be published. doi: 10.1109/TPEL.2019.2933664.

[14] X. Sun, Y. Shen, S. Wang, G. Lei, Z. Yang, and S. Han, "Core losses analysis of a novel 16/10 segmented rotor switched reluctance BSG motor for HEVs using nonlinear lumped parameter equivalent circuit model," *IEEE/ASME Trans. Mechatronics*, vol. 23, no. 2, pp. 747–757, Apr. 2018.

[15] X. Sun, K. Diao, and Z. Yang, "Performance improvement of a switched reluctance machine with segmental rotors for hybrid electric vehicles," *Comput. Elect. Eng.*, vol. 77, pp. 244–259, Jun. 2019.

[16] T. Hiromi, T. Katou, A. Chiba, M. A. Rahman, and T. Fukao, "A novel magnetic suspension-force compensation in bearingless induction-motor drive with squirrel-cage rotor," *IEEE Trans. Ind. Appl.*, vol. 43, no. 1, pp. 66–76, Jan. 2007.

[17] A. Chiba and J. A. Santisteban, "A PWM harmonics elimination method in simultaneous estimation of magnetic field and displacements in bearingless induction motors," *IEEE Trans. Ind. Appl.*, vol. 48, no. 1, pp. 124–131, Jan./Feb. 2012.

[18] T. Tera, Y. Yamauchi, A. Chiba, T. Fukao, and M. A. Rahman, "Performances of bearingless and sensorless induction motor drive based on mutual inductances and rotor displacements estimation," *IEEE Trans. Ind. Electron.*, vol. 53, no. 1, pp. 187–194, Feb. 2005.

[19] X. Sun, C. Hu, G. Lei, Y. Guo, and J. Zhu, "State feedback control for a PM hub motor based on grey wolf optimization algorithm," *IEEE Trans. Power Electron.*, to be published. doi: 10.1109/TPEL.2019.2923726.

[20] Z. Shi, X. Sun, Y. Cai, Z. Yang, G. Lei, Y. Guo, and J. Zhu, "Torque analysis and dynamic performance improvement of a PMSM for EVs by skew angle optimization," *IEEE Trans. Appl. Supercond.*, vol. 29, no. 2, Mar. 2019, Art. no. 0600305.

[21] X. Sun, C. Hu, J. Zhu, S. Wang, W. Zhou, Z. Yang, G. Lei, K. Li, B. Zhu, and Y. Guo, "MPTC for PMSMs of EVs with multi-motor driven system considering optimal energy allocation," *IEEE Trans. Magn.*, vol. 55, no. 7, 2019, Art. no. 8104306.

[22] A. Smirnov, A. H. Pesch, O. Pyrhönen, and J. T. Sawicki, "High-precision cutting tool tracking with a magnetic bearing spindle," *J. Dyn. Syst., Meas. Control*, vol. 137, no. 5, 2015, Art. no. 051017.

[23] A. H. Pesch, A. Smirnov, O. Pyrhönen, and J. T. Sawicki, "Magnetic bearing spindle tool tracking through μ-synthesis robust control," *IEEE/ASME Trans. Mechatronics*, vol. 20, no. 3, pp. 1448–1457, Jun. 2015.

[24] X. D. Sun, Z. Shi, Z. B. Yang, S. H. Wang, B. K. Su, L. Chen, and K. Li, "Digital control system design for bearingless permanent magnet synchronous motors," *Bull. Pol. Acad. Sci.-Tech. Sci.*, vol. 66, no. 5, pp. 687–698, Oct. 2018.

[25] S. M. Ahmad, O. A. Ahmed, Z. Mohamed. "Vibration induced failure analysis of a high speed rotor supported by active magnetic bearings," *Trans. Can. Soc. Mech. Eng.*, vol. 39, no. 4, pp. 855–866, 2015.

[26] X. Sun, B. Su, L. Chen, Z. Yang, X. Xu, and Z. Shi, "Precise control of a four degree-of-freedom permanent magnet biased active magnetic bearing system in a magnetically suspended direct-driven spindle using neural network inverse scheme," *Mech. Syst. Signal Process.*, vol. 88, pp. 36–48, May 2017.

[27] Z. Jin, X. Sun, Z. Yang, S. Wang, L. Chen, and K. Li, "A novel four degree-of-freedoms bearingless permanent magnet machine using modified cross feedback control scheme for flywheel energy storage systems," *Int. J. Appl. Electromagn. Mech.*, vol. 60, no. 3, pp. 379–392, 2019.

[28] X. Sun, L. Chen, Z. Yang, and H. Zhu, "Speed-sensorless vector control of a bearingless induction motor with artificial neural network inverse speed observer," *IEEE/ASME Trans. Mechatronics*, vol. 18, no. 4, pp. 1357–1366, Aug. 2013.

[29] C. H. Park, S. K. Choi, and S. Y. Ham, "Design of magnetic bearings for turbo refrigerant compressors," *Mech. Ind.*, vol. 15, no. 4, pp. 245–252, 2014.

[30] X. Sun, L. Chen, H. Jiang, Z. Yang, J. Chen, and W. Zhang, "High-performance control for a bearingless permanent-magnet synchronous motor using neural network inverse scheme plus internal model controllers," *IEEE Trans. Ind. Electron.*, vol. 63, no. 6, pp. 3479–3488, Jun. 2016.

[31] C.-K. Chen and T. D. Chu, "Nonlinear modeling and control of active magnetic bearings for a flywheel energy storage system," in *Proc. 6th Int. Conf. Intell. Hum.-Mach. Syst. Cybern.*, Hangzhou, China, 2014, pp. 284–287.

[32] R. Schöb, C. Redemann, and T. Gemmp, "Radial active magnetic bearing for operation with 3-phase power converter," in *Proc. 4th Int. Symp. Magn. Suspension Technol.*, Gifu, Japan, 1997, pp. 111–124.

[33] X. Sun, Z. Shi, L. Chen, and Z. Yang, "Internal model control for a bearingless permanent magnet synchronous motor based on inverse system method," *IEEE Trans. Energy Convers.*, vol. 31, no. 4, pp. 1539–1548, Dec. 2016.

[34] J. Asama, M. Amada, N. Tanabe, N. Miyamoto, A. Chiba, S. Iwasaki, M. Takemoto, T. Fukao, and M. A. Rahman, "Evaluation of a bearingless PM motor with wide magnetic gaps," *IEEE Trans. Energy Convers.*, vol. 25, no. 4, pp. 957–964, Dec. 2010.

[35] Q. D. Nguyen and S. Ueno, "Modeling and control of salient-pole permanent magnet axial-gap self-bearing motor," *IEEE Trans. Magn.*, vol. 16, no. 3, pp. 518–526, Jun. 2011.

[36] X. Sun, B. Su, L. Chen, Z. Yang, and K. Li, "Design and analysis of interior composite-rotor bearingless permanent magnet synchronous motors with two layer permanent magnets," *Bull. Polish Acad. Sci., Tech. Sci.*, vol. 65, no. 6, pp. 833–843, 2017.

[37] M. Ooshima *et al.*, "Performance evaluation and test results of a 11 000 r/min, 4 kW surface-mounted permanent magnet-type bearingless motor," in *Proc. 7th Int. Symp. Magn. Bearings*, Zurich, Switzerland, 2000, pp. 377–382.

[38] T. Reichert, T. Nussbaumer, and J. W. Kolar, "Bearingless 300-W PMSM for bioreactor mixing," *IEEE Trans. Ind. Electron.*, vol. 59, no. 3, pp. 1376–1388, Mar. 2012.

[39] X. Sun, B. Su, S. Wang, Z. Yang, G. Lei, J. Zhu, and Y. Guo, "Performance analysis of suspension force and torque in an IBPMSM with V-shaped PMs for flywheel batteries," *IEEE Trans. Magn.*, vol. 54, no. 11, Nov. 2018, Art. no. 8105504.
[40] T. Reichert, T. Nussbaumer, W. Gruber, and J. W. Kolar, "Bearingless permanent-magnet motor with 4/12 slot-pole ratio for bioreactor stirring applications," *IEEE Trans. Ind. Mechatronics*, vol. 16, no. 3, pp. 431–439, Jun. 2011.
[41] T. Zhang, W. Ni, X. Wang, C. Zhang, and H. Jia, "Optimal design on bearingless permanent magnet synchronous motor to decrease losses and torque ripple," *Sensors Transducers*, vol. 182, no. 11, pp. 138–145, 2014.
[42] H.-W. Cho, H.-K. Sung, J.-Y. Choi, D.-J. You, J.-H. Park, S.-M. Jang, and S.-H. Lee, "Analytical calculation of rotor losses in high-speed permanent magnet synchronous motor at different load conditions," *J. Appl. Phys.*, vol. 103, no. 7, pp. 07F129-1–07F129-3, 2008.
[43] M. Oshima, S. Miyazawa, T. Deido, A. Chiba, F. Nakamura, and T. Fukao, "Characteristics of a permanent magnet type bearingless motor," *IEEE Trans. Ind. Appl.*, vol. 32, no. 2, pp. 363–370, Mar. 1996.
[44] Z. Huangqiu and Z. Tao, "Finite element analysis on permanent magnet synchronous motor," (in Chinese), *Proc. CSEE*, vol. 3, no. 25, pp. 136–140, 2006.
[45] S. Dwari and L. Parsa, "Design of Halbach-array-based permanent-magnet motors with high acceleration," *IEEE Trans. Ind. Electron.*, vol. 58, no. 9, pp. 3768–3775, Sep. 2011.
[46] L. Zhang, B. Kou, F. Xing, and H. Zhang, "Analysis and comparison of two two-dimensional Halbach permanent magnet arrays for magnetically levitated planar motor," *J. Appl. Phys.*, vol. 115, no. 17, pp. 17E704-1–17E704-3, 2014.
[47] S. Sadeghi and L. Parsa, "Multiobjective design optimization of five-phase Halbach array permanent-magnet machine," *IEEE Trans. Magn.*, vol. 47, no. 6, pp. 1658–1666, Jun. 2011.
[48] R. P. Praveen, M. H. Ravichandran, V. T. S. Achari, V. P. J. Raj, G. Madhu, and G. R. Bindu, "A novel slotless Halbach-array permanent-magnet brushless DC motor for spacecraft applications," *IEEE Trans. Ind. Electron.*, vol. 59, no. 9, pp. 3553–3560, Sep. 2012.

TAO ZHANG was born in Huai'an, China, in 1978. He received the B.S. and M.S. degrees in power electronic and power transmission from Jiangsu University, Zhenjiang, China, in 2001 and 2006, respectively, and the Ph.D. degree in electrical engineering from Jiangsu University, in 2012. He is currently an Assistant Professor with the Huaiyin Institute of Technology. He is also a Researcher with the Jiangsu Engineering Research Center on Meteorological Energy Using and Control, Nanjing University of Information Science and Technology, Nanjing, China. His current research interests include beaingless motors, magnetic bearings, high speed motors, and control strategies.

XIAOTING YE was born in Huai'an, China, in 1981. She received the B.S. degree in electrical engineering and the M.S. degree in detection technology and automation from the China University of Mining and Technology, Xuzhou, China, in 2003 and 2006, respectively. Her research interests include magnetic bearings, bearingless motors, and nonlinear intelligent control of motors.

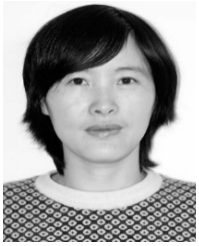

LIHONG MO received the M.S. degree in electrical engineering from the Anhui University of Science and Technology, Huainan, China, in 2005, and the Ph.D. degree in electrical engineering from Jiangsu University, Zhenjiang, China, in 2015. She is currently an Assistant Professor with the Huaiyin Institute of Technology. Her research interests include permanent magnet machine design, modeling, and control.

QING LU received the B.S. degree from Hangzhou Dianzi University, Hangzhou, China, in 2003, and the M.S. degree from the China University of Mining and Technology, Xuzhou, China, in 2008. He is currently pursuing the Ph.D. degree with Jiangsu University, Zhenjiang, China. He is currently a Lecturer with the Faculty of Automation, Huaiyin Institute of Technology. His main research interests include electric drive and the control of permanent magnet motors.